Received: 15 March 2018 | Revised: 31 July 2018 | Accepted: 6 August 2018

DOI: 10.1002/poc.3896

RESEARCH ARTICLE

WILEY Journal of Physical Organic Chemistry

Photophysical insights and guidelines for blue "turn-on" fluorescent probes for the direct detection of nitric oxide (NO•) in biological systems

Mina Barzegar Amiri Olia[1] | Amber N. Hancock[1] | Carl H. Schiesser[2] | Lars Goerigk[3] | Uta Wille[1]

[1]School of Chemistry, Bio21 Institute, The University of Melbourne, Parkville, Victoria, Australia

[2]Seleno Therapeutics Pty Ltd, Brighton East, Victoria, Australia

[3]School of Chemistry, The University of Melbourne, Parkville, Victoria, Australia

Correspondence
Lars Goerigk, School of Chemistry, The University of Melbourne, Parkville, Victoria 3010, Australia.
Email: lars.goerigk@unimelb.edu.au

Uta Wille, School of Chemistry, Bio21 Institute, The University of Melbourne, Parkville, Victoria 3010, Australia.
Email: uwille@unimelb.edu.au

Funding information
National Computational Infrastructure; Victorian Life Sciences Computation Initiative; High Performance Computing Facility of the University of Melbourne; Discovery Scheme, Grant/Award Number: DP13010007; Centres of Excellence Scheme, Grant/Award Number: CE0561607; Australian Research Council, Grant/Award Numbers: CE0561607, DE140100550 and DP13010007; University of Melbourne

Abstract

Synthesis and photophysical properties of a family of five blue fluorescent "turn-on" probes for the direct detection of nitric oxide (NO•) is reported. The probes **CB1-5** feature a substituted 7-hydroxy coumarin chromophore coupled to 2-methyl-8-aminoquinoline, which act as tridentate ligand for Cu(II) and active site for monitoring NO• using a replacement strategy. The UV/vis absorption and fluorescence emission characteristics of the probes are significantly influenced by the substitution pattern on the coumarin ring, as well as by solvent polarity and pH. Time-dependent density functional theory (TD-DFT) calculations for **CB4** and **CB5** showed that the absorptions are due to π-π* transitions localised on coumarin, with a small charge transfer contribution from the quinoline system at higher pH where the 7-hydroxy coumarin moiety is deprotonated, which leads to a bathochromic shift of the absorption. Complexation of the probes with Cu(II) quenches the fluorescence, which is turned back on upon reaction with NO•, allowing selective detection of this important signalling molecule in μM concentrations. Preliminary experiments revealed that **CB4** and **CB5** enable to monitor endogenously produced NO• in living bacterial cells in multi-dye imaging experiments.

KEYWORDS

density functional theory calculations, fluorescent probes, multi-dye imaging, nitric oxide, photophysical studies

1 | INTRODUCTION

The free radical species nitric oxide (NO•) is an important signalling molecule, which is produced by many cell types in a variety of tissues. For example, NO• is generated during immune and inflammatory responses[1] and is essential for the regulation of various physiological processes, including cardiovascular function.[2] Recently, NO• was also identified as a key regulator for the dispersal of bacterial biofilms.[3] Biofilms are compact colonies of microorganisms that grow on living and non-living surfaces and cause serious problems, for example in industrial environments[4] and hospitals,[5] as well as in cultural materials conservation.[6] Biofilms are held together by a matrix of extracellular polymeric materials consisting of DNA, polysaccharides, and proteins, which

preserve nutrients and obstruct the diffusion of antibacterial agents.[7,8] Thus, biofilm-based bacteria display an increased resistance to treatment and are less vulnerable to antibacterial agents compared with planktonic suspensions.[7,9] Complete eradication of bacterial biofilms is extremely difficult and often not feasible, in particular when damage of the underlying surface must be avoided.[10] Inhibition of biofilm formation and biofilm cell dispersal are the most common non-invasive approaches for biofilm removal to date.[11] Since the discovery that NO• triggers a regulated and coordinated dispersal of bacterial biofilms, NO• donor compounds have been successfully employed to initiate biofilm breakdown. It is during the transition of the sessile biofilm colony into free-swimming planktonic cells that biofilms become vulnerable to remediation.[12,13]

Remarkably, the mechanism by which NO• mediates formation and dispersal of biofilms is still not fully understood. The development of new approaches for the efficient eradication of biofilms requires the availability of methods to detect NO• in biological systems with high sensitivity and selectivity, and a number of sensors based on electrochemical[14] and fluorescence[15] methods have been invented. Fluorescence techniques in combination with laser-scanning confocal microscopy are particularly powerful approaches due to the high spatiotemporal resolution.[16] The ideal sensor for detecting NO• in biological systems should have a very high fluorescence emission at physiological pH for maximum sensitivity. The majority of the currently available fluorescent probes for NO• emit in the green or red region of the electromagnetic spectrum,[17] which is, unfortunately, also the region where most of the DNA, protein, or other cell function fluorescence stains are emitting. Thus, in order to enable visualisation of the site of NO• production in cells simultaneously with other cell constituents, the development of sensitive NO• selective probes that fluoresce in the blue region (λ_{em} ~ 470 ± 25 nm) and which could be used in multi-dye imaging experiments is highly desirable.

Lippard et al developed a strategy to transform fluorophores into sensors for NO•, which utilises a non-fluorescent copper complex that turns on fluorescence upon replacement of the metal by NO•.[17,18] If coumarin and its derivatives, which are known blue-fluorescent dyes,[19] would be used as chromophore, some of us recently suggested that Lippard's replacement approach could provide access to blue "turn-on" fluorescent probes and hereupon synthesised the probe **CB5** to test its potential to detect NO•(Scheme 1).[20]

In **CB5**, a substituted coumarin is linked to 2-methyl-8-aminoquinoline to provide a tridentate ligand for Cu(II).[18] Treatment of **CB5** with Cu(II) produces the complex **Cu(II)-CB5** in which fluorescence is quenched, presumably by the paramagnetic Cu(II) ion.[18,21] It was pleasing to see that reaction of **Cu(II)-CB5** with NO• leads to replacement of the metal ion through a redox reaction, which results in formation of the *N*-nitrosamine **CB5-NO** and blue fluorescence turn-on.[20]

In our previous work, we did not explore the photophysical properties of the probe. However, fundamental knowledge whether and how the substitution pattern at the coumarin chromophore affects the UV/vis absorption and fluorescence emission behaviour is essential to guide the design and development of selective and sensitive blue "turn-on" fluorescence sensors for NO• in the future. In this work, we will close this gap by providing a detailed assessment of the performance of a series of five coumarin-based fluorescent probes (**CB1-5**), which all contain a 2-methyl-8-aminoquinoline moiety as coordination site for Cu(II) but differ in the substitution pattern on the coumarin ring. The photophysical studies are augmented with TD-DFT calculations to obtain understanding of the nature of the electronic transitions in these compounds. Furthermore, we also explored the selectivity of the probes for NO• and performed preliminary multi-dye fluorescence imaging studies to visualise endogenously produced NO• in living bacterial cells.

2 | RESULTS AND DISCUSSION

2.1 | Synthesis of the probes CB1-5

Scheme 2 outlines the synthetic strategy to access the functionalized coumarin dyes **CB1-5**. Briefly, the coumarin chromophores **1a,c-d** were synthesised through a Knoevenagel reaction involving 2,4-dihydroxy benzaldehydes and substituted malonates or phenylacetic acid,

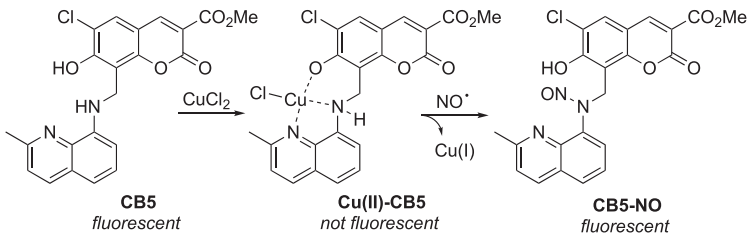

SCHEME 1 Mechanism of "turn-on" fluorescence through replacement of Cu(II) by NO• in the recently developed coumarin based probe **CB5**[20]

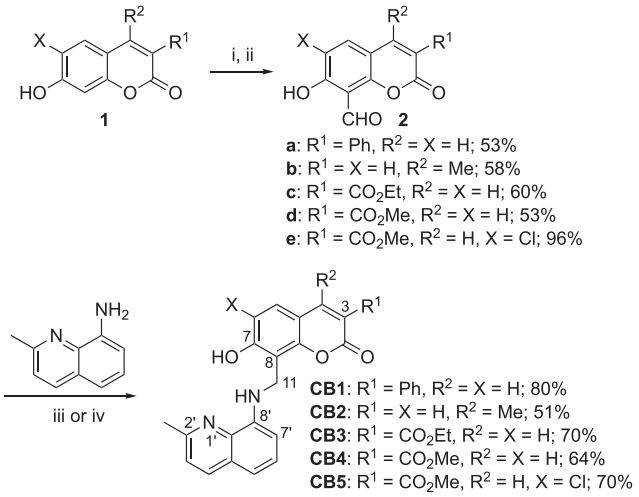

SCHEME 2 *Reagents and conditions:* (i) Hexamine, TFA, reflux, 20 h. (ii) Hexamine, HOAc, 70°C, 6 h. (iii) MeOH, MS (4 Å), rt, 8 h, then $NaBH_4$, 24 h, rt. (iv) MeOH, CH_2Cl_2, MS (4 Å) rt, 8 h, then Na $(OAc)_3BH$, 24 h, rt.

respectively.[22] Formylation at C-8 through a Duff reaction in the presence of trifluoroacetic acid and hexamine gave aldehydes **2a-e**,[23] which were coupled to 2-methyl-8-aminoquinoline via an intermediate Schiff base, followed by reduction to yield **CB1-5**.[18,20] Details are given in the Experimental Section (see also Figures S1-12 in the Supporting Information, SI).

2.2 | Photophysical properties of CB1-5 in the absence of Cu(II) and NO•

The photophysical properties of the probes were explored using 100 μM of **CB1-5** in aqueous buffer solution at pH 7 (tris-buffered saline (TBS) with 1% DMSO; details of the sample preparation are given in the Experimental Section). The absorption and emission characteristics of all compounds are compiled in Table 1. The spectra are shown in Figure S13.

TABLE 1 Absorption and emission maxima (in nm) and pK_a values of **CB1-5** (100 μM in TBS at pH 7, with 1% DMSO)

Compound	$\lambda_{abs,max}$[a]	λ_{ex}[b]	$\lambda_{em,max}$[c]	pK_a
CB1	355	350	489	9.5
CB2	339	325	470	8
CB3	363, 412	350, 410	450	7.4
CB4	366, 409	360, 410	450	7
CB5	410	420	448	4

[a]Maximum absorbance.

[b]Excitation wavelength.

[c]Maximum fluorescence emission.

The phenyl substituted probe **CB1** has a fluorescence maximum at λ = 489 nm, which lies in the green-blue region of the UV/vis spectrum and is not suitable for monitoring NO• in the intended multi-dye imaging experiments. Replacing the phenyl group at C-3 by a methyl group at C-4 blue shifts the emission band to λ = 470 nm (**CB2**). Unfortunately, the absorption band also shifts to a shorter wavelength to appear at λ = 339 nm, which is not compatible with experiments in living cells. On the other hand, having no substituent at C-4 in coumarin but electron-withdrawing ester groups at C-3 (**CB3**, **CB4**, and **CB5**) maintains blue fluorescence emission at λ ~ 450 nm, while red-shifting the absorption maximum to λ ~ 410 nm. Thus, the probes **C3-C5** could be excited with a laser at λ = 405 nm in the confocal microscope without adverse impact on cells.[20,24]

Interestingly, at pH 7, both **CB3** and **CB4** display two absorption bands, but excitation at either of these bands resulted in similar fluorescence emission spectra. 7-Hydroxy coumarin dyes are known to exhibit pH-responsive and solvent-responsive, ratio-metric absorption/excitation profiles as a result of the equilibrium between the neutral phenol moiety and the phenolate anion.[25] We therefore investigated the effect of pH and solvent on $\lambda_{abs,max}$ of our probes in more detail. The pK_a values for **CB1-5** were determined from the UV/vis absorbance as a function of pH (see Figure S14) and are included in Table 1. Table 2 presents the $\lambda_{abs,max}$ data for all probes at selected pH as well as in several non-aqueous solvents. The UV/vis absorption spectra are shown in Figures S15 and S16.

While the pK_a of phenyl-substituted **CB1** (9.5) is similar to that of phenol, the strong electron-withdrawing ester substituents at C-3 on the coumarin moiety increase the acidity of the hydroxyl group by about two orders of magnitude. Additional electron-withdrawing substituents at C-6 (*ortho* to OH), for example chlorine in **CB5**, lead to a further increase of the acidity by three orders of magnitude.

The different acidity of the various probes is reflected in the absorption spectra. No noticeable change between pH 1 and 8 was found for **CB1**, which exhibits one absorbance band with a maximum at λ ~ 355 nm. Increasing the pH to 11 leads to a bathochromic shift of the absorption maximum to λ = 396 nm, which is due to deprotonation of the phenolic hydroxyl group. For **CB2**, a similar gradual red shift of the absorption maximum from λ = 326 nm at pH 3 to λ = 367 nm at pH 11 was found. The more acidic **CB3** and **CB4** display only one absorption band with λ_{max} ~ 355 nm at pH 1-5. Increasing the pH to 7-8 produces a second absorption maximum at λ = 412 nm and λ = 409 nm respectively, which becomes the sole absorption peak at pH 11, where the phenolic

TABLE 2 Effect of pH and solvent on the UV/Vis absorption maxima $\lambda_{abs,max}$ (in nm) of **CB1-5** (100-μM solutions)

Solvent	CB1	CB2	CB3	CB4	CB5
pH 1[a]	350	n.d.[b]	354	352	356
pH 3[a]	352	326	355	354	362
pH 5[a]	354	n.d.	360	360	410
pH 7[a]	355	339	363, 412[c]	366, 409[c]	410
pH 8[a]	358	345	413	370[c], 411	n.d.
pH 11[a]	396	367	413	411	410
DMSO	348, 445	325, 390	358, 436	356, 441	357, 440
MeOH	343	n.d.	359, 419	360, 417	357, 417
EtOH	343	327	353, 414	362, 420	n.d.
Et_2O	347	n.d.	351	355	354, 438
MeCN	342	321	349, 427	356, 429	353, 435

[a]In TBS with 1% DMSO.

[b]n.d. = not determined.

[c]Peak appeared as a shoulder.

OH group is fully deprotonated in both probes. **CB5**, the most acidic compound in this series (pK_a = 4), exhibits one absorption band with λ_{max} ~ 360 nm under very acidic conditions (pH 1-3), which red shifts to λ_{max} = 410 nm at pH 5 with no further changes at higher pH. This clearly shows that **CB5** is fully deprotonated at physiological pH.

Table 2 also reveals significant solvent effects on $\lambda_{abs,max}$. Thus, the absorption maximum of **CB1** in MeOH, EtOH, Et_2O, and MeCN is the same as in aqueous buffer at pH 1-8. However, **CB1** exhibits in DMSO not only a band with λ_{max} = 348 nm (corresponding to "neutral" **CB1**), but also a second, red-shifted band centred at λ = 445 nm. A similar solvent effect was also observed for **CB2**, where a second, red-shifted absorption in DMSO appears with λ_{max} = 390 nm. Interestingly, **CB3** and **CB4** exhibit a second bathochromic absorption band not only in DMSO, but also in MeCN, EtOH, and MeOH, which red-shifts in the order MeOH/EtOH < MeCN < DMSO. No such solvent effect was observed for the absorption band that can be assigned to the "neutral" **CB3** and **CB4**. In contrast to this, **CB5** displays two absorption maxima in all organic solvents. Apart from the absorption band of the neutral species centred at λ ~ 355 nm and which does not significantly vary with solvent, a second red-shifted absorption appears at λ_{max} = 417 nm in MeOH and at λ_{max} = 435-440 nm in Et_2O, DMSO, and MeCN. This second, bathochromically shifted band in **CB1-5** could result from a solvent-induced ground state deprotonation. A similar solvent dependence of λ_{max} has been described for 3-hydroxyflavone[26] and coumarin-substituted nicotinamides.[27] The extent of the solvochromatic shift correlates with the pK_a for **CB1-5**. In the case of the least acidic coumarin derivative **CB1**, this effect is only observed with the most polar solvent DMSO, while the strongly acidic **CB5** interacts with DMSO, MeOH, MeCN, and even Et_2O.[28]

Since it is known that the fluorescence emission intensity of unsubstituted 7-hydroxycoumarin is also pH dependent,[29] we next explored the effect of pH on the fluorescence emission spectra of **CB1-5**. As expected, in aqueous solution, the emission intensities of all probes increased with increasing pH due to progressive deprotonation (see Figure S17 for **CB1-4**). Figure 1 shows the fluorescence emission of **CB1-5** at pH 7, which clearly reveals a significantly higher emission intensity for **CB5** compared with **CB1-4**.

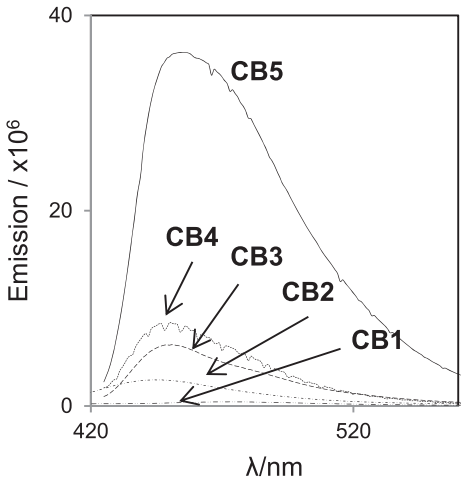

FIGURE 1 Fluorescence emission intensities of **CB1-5** at pH 7 (100 μM in TBS, with 1% DMSO; λ_{ex} = 410 nm (**CB1,3-5**) or 360 nm (**CB2**))

This finding can be rationalised by the degree of deprotonation of the probes at pH 7. **CB1** and **CB2** are fully protonated and show only weak fluorescence. **CB3** and **CB4** are partially deprotonated, leading to a more intense fluorescence emission. **CB5** exists exclusively as the phenolate at pH 7, which clearly shows that the observed strong fluorescence emission is due to the *O*-deprotonated coumarin. Therefore, with regards to the intended detection of NO• in biological systems, **CB5** appears particularly promising: (1) because of the complete deprotonation of the coumarin moiety the fluorescence intensity is the highest at physiological pH, which makes **CB5** the most sensitive probe of those studied here; and (2) the absorption maximum of $\lambda_{max} = 410$ nm remains constant above pH 5 (in contrast to **CB1-4**), which enables examination by confocal laser-scanning microscopy through excitation with a 405-nm laser. Overall, these data show that blue coumarin based "turn-on" fluorescent probes for NO• require electron-withdrawing substituents at C-3 and C-6 on the coumarin ring system to ensure full deprotonation of the phenolic hydroxyl group at physiological pH for high sensitivity.

The influence of the organic solvent on the fluorescence emission $\lambda_{em,max}$ was more subtle and is shown in Table 3 exemplary for **CB1** and **CB4**. Overall, the fluorescence emission intensity of **CB1** is considerably stronger in DMSO than in any other organic solvent investigated in this work (see Figure S18). Compared with the band at pH 7 in aqueous solution (see Table 1), $\lambda_{em,max}$ becomes slightly blue-shifted by up to 20 nm in organic solvents without any obvious dependence on solvent polarity. Compared with **CB1**, the fluorescence emission intensity of the more acidic **CB4** is higher in the most polar solvents explored here (ie, EtOH, MeOH, DMSO; see Figure S18), but only a very small solvent variability of $\lambda_{em,max}$ was found, except for Et_2O, where **CB4** exhibits a second, red-shifted emission band with $\lambda_{max} = 547$ nm. However, since Et_2O is not a suitable solvent for studies in biological systems, we did not further investigate this effect.

In comparison with **CB1**, the generally higher fluorescence emission intensities of **CB4** in organic solvents might be due to the solvent-induced ground state deprotonation proposed above (see Table 2) or could suggest a rapid deprotonation within the lifetime of its singlet excited state. In fact, it is known that the pK_a value of phenols decreases by several orders of magnitude upon electronic excitation, likely due to charge redistribution, which is stabilised by polar solvents.[29,30] Overall, these findings confirm the observations made above that the observed fluorescence arises from probes with an *O*-deprotonated coumarin moiety.

TABLE 3 Solvent effect on the fluorescence emission maxima $\lambda_{em,max}$ (in nm) of **CB1** and **CB4** (100 μM solutions; $\lambda_{ex} = 410$ nm)

Solvent	CB1	CB4
DMSO	490	462
MeOH	478	450
EtOH	478	452
MeCN	485	450
EtOAC	487	449
$CHCl_3$	477	449
Et_2O	473	451, 547
THF	486	450

3 | COMPUTATIONAL STUDIES

In order to obtain a fundamental understanding of the observed absorption and emission properties, DFT calculations were exemplary performed for **CB4** and **CB5** in their neutral and anionic (ie, phenolate) states, as well as for three different *N*-protonated forms (Figure 2). *N*-Protonated derivatives were included in the computational studies to explore whether such compounds could contribute to the observed UV/vis absorption spectra under very acidic conditions.

We first performed a thorough conformational search with reliable dispersion-corrected DFT techniques (see Computational Methods for details), followed by linear-response TD-DFT treatments. The latter were carried out with the range-separated hybrid DFT approximation CAM-B3LYP[31] and the 6-311G**[32] atomic-orbital (AO) basis set. This method has been shown to be reliable for the calculation of vertical singlet-singlet excitation energies in medium-sized organic dyes[33] and is sufficiently accurate to provide a qualitative analysis of the systems explored in this study. The first seven excitation

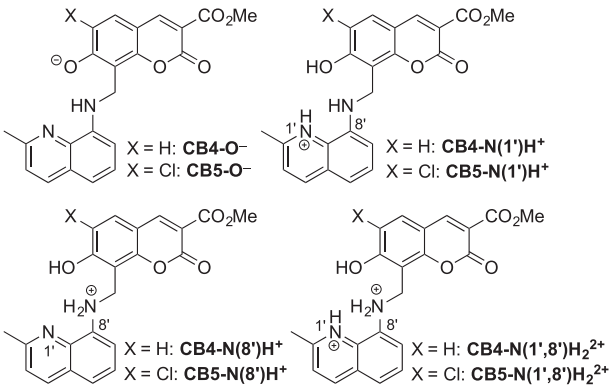

FIGURE 2 *O*-deprotonated and *N*-protonated isomers of **CB4** and **CB5**

energies were calculated together with their oscillator strengths (f). These results were used to simulate the UV/vis absorption spectra. Details are given in the Computational Methods section.

Comparison of the simulated spectra for different conformers of the various protonation states of **CB4** and **CB5** revealed similarity in the absorption range of interest. Therefore, it is unlikely that the observed spectral features shown in Tables 1 and 2 can be explained with contributions stemming from different conformers of **CB4** and **CB5**, respectively (see Figures S19-S21). The role of the solvent was studied by performing calculations for the gas phase and for DMSO, H_2O, and MeOH, using a continuum solvation model (see Computational Methods for details), but no considerable differences for the gas phase and in solution were found (see Figure S22). This result could indicate that continuum solvation models may not describe all possible solvent effects adequately when **CB4,5** is the solute. However, it should be noted that explicit solvation was not explored in this work, because we were interested in obtaining a qualitative understanding rather than a detailed characterisation of the role of solvent on the electronic transitions. Furthermore, since the calculated data for **CB4** and **CB5** were very similar, we will restrict the following discussion to **CB5** using DMSO as the solvent.

Figure 3 shows the computed lowest-energy conformations for the neutral (**CB5**), deprotonated (**CB5-O$^-$**) and the different protonated forms (**CB5-N(1′)H$^+$**, **CB5-N(8′)H$^+$**, and **CB5-N(1′,8′)H$_2^{2+}$**). A significant change of the relative arrangement between the coumarin and quinoline moieties in dependence of the protonation state is apparent. While in neutral **CB5** hydrogen bonding between the coumarin OH and the NH group at C-8′ in quinoline leads to a twisted arrangement of the two aromatic ring systems that can be characterised by the dihedral angle *d*(8, 11, 8′, 7′) of 51°, lack of such hydrogen bonding in the phenolate **CB5-O$^-$** puts the planes of the coumarin and quinoline rings nearly orthogonal with *d*(8, 11, 8′, 7′) = 80°. The geometries of the *N*-protonated derivatives are governed by various hydrogen bonds between NH groups and the lactone moiety in coumarin, causing rotation of the quinoline framework towards coumarin. It should be noted that protonation of the NH group at C-8′ in quinoline leads to considerable elongation of the C(11)-N bond by about 0.06 Å (in **CB5-N(8′)H$^+$**) or by 0.09 Å (in **CB5-N(1′,8′)H$_2^{2+}$**) compared with **CB5-N(1′)H$^+$**. Both singly protonated forms can be

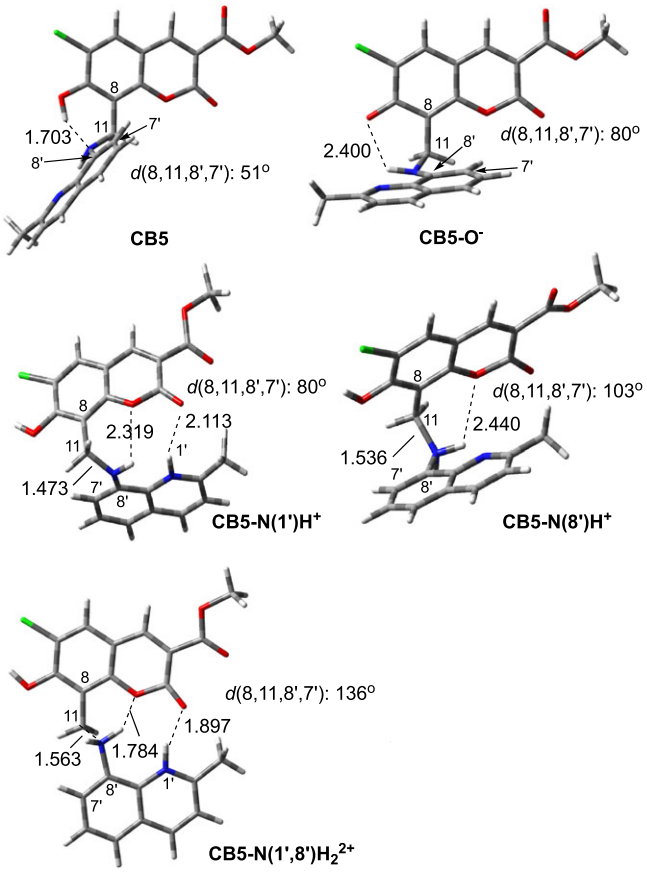

FIGURE 3 Calculated lowest-energy conformations for the different protonation states in **CB5**, optimised at the TPSS-D3/def2-TZVP level of theory; distances in A; *d* = dihedral angle (for atom numbering see also Scheme 2)

described as a folded conformer with favourable dispersion interactions between the two aromatic moieties.

In order to predict the preferred *N*-protonation site, we determined the adiabatic proton affinities (PA) from the energies of the two singly protonated species relative to the neutral system (see Computational Methods). For the formation of **CB5-N(1′)H$^+$**, a value of PA = −247.1 kcal mol^{-1} was obtained, which is 7.5 kcal mol^{-1} lower in energy than the value for the formation of **CB5-N(8′)H$^+$** (PA = −239.6 kcal mol^{-1}). The calculated more favourable protonation of the ring nitrogen agrees well with the experimentally determined higher basicity (pKa = 4.94),[34] compared with the exocyclic amino group in 8-amino quinoline (pKa ~ 3.05).[35]

According to the computations, the first absorption band of **CB5** has the highest oscillator strength of f = 0.660 and an excitation energy of 3.80 eV (λ_{max} = 326 nm). The dominant contribution to λ_{max} is a transition from a π orbital (HOMO-1 for our chosen level of theory) to a π^* orbital (LUMO), which are both localised on the coumarin system (Figure 4A), and where "HOMO" stands for the highest occupied molecular orbital and "LUMO" for the lowest unoccupied molecular orbital.

In the case of **CB5-O$^-$**, the strongest transition has an oscillator strength of f = 0.758 with an excitation energy of 3.38 eV, which corresponds to λ_{max} = 366 nm. Interestingly, the HOMO-1 in **CB5-O$^-$** is delocalized over both coumarin and quinoline moieties, whereas the LUMO is localised on coumarin only (Figure 4B). This indicates a small CT contribution to the transition, which leads to a bathochromic shift in the UV/vis spectrum of about 0.41 eV (ca. 40 nm) compared with the neutral **CB5**. This finding is in very good qualitative agreement with the experimentally found red shift of 0.46 eV (ca. 50 nm) for the absorption maximum of **CB5** at pH > 5 (see Table 2), which can therefore be clearly assigned as **CB5-O$^-$**.

Figure 5A compares the simulated UV/vis spectra for **CB5** and **CB5-O$^-$** with the experimentally determined spectra at pH 1 and 7. The computed spectra are 0.30 to 0.37 eV blue-shifted compared with the experimentally determined data. The expected average error for TD-CAMB3LYP is about 0.2 eV,[29] while errors for the PCM continuum solvation model can vary between 0.05 and 0.1 eV.[37] Our computational results are therefore in excellent agreement with the reported accuracy for this method and enable to obtain a reliable qualitative understanding of these systems.[38]

The major contributions to λ_{max} differ partially among the three *N*-protonated forms. While all three forms are characterised by π-π^* transitions, we observe only for **CB5-N(8′)H$^+$** that the involved MO pair is localised entirely on the coumarin moiety (Figure 4D). The excitations for **CB5-N(1′)H$^+$** and **CB5-N(1′,8′)H$_2^+$** involve MOs that are

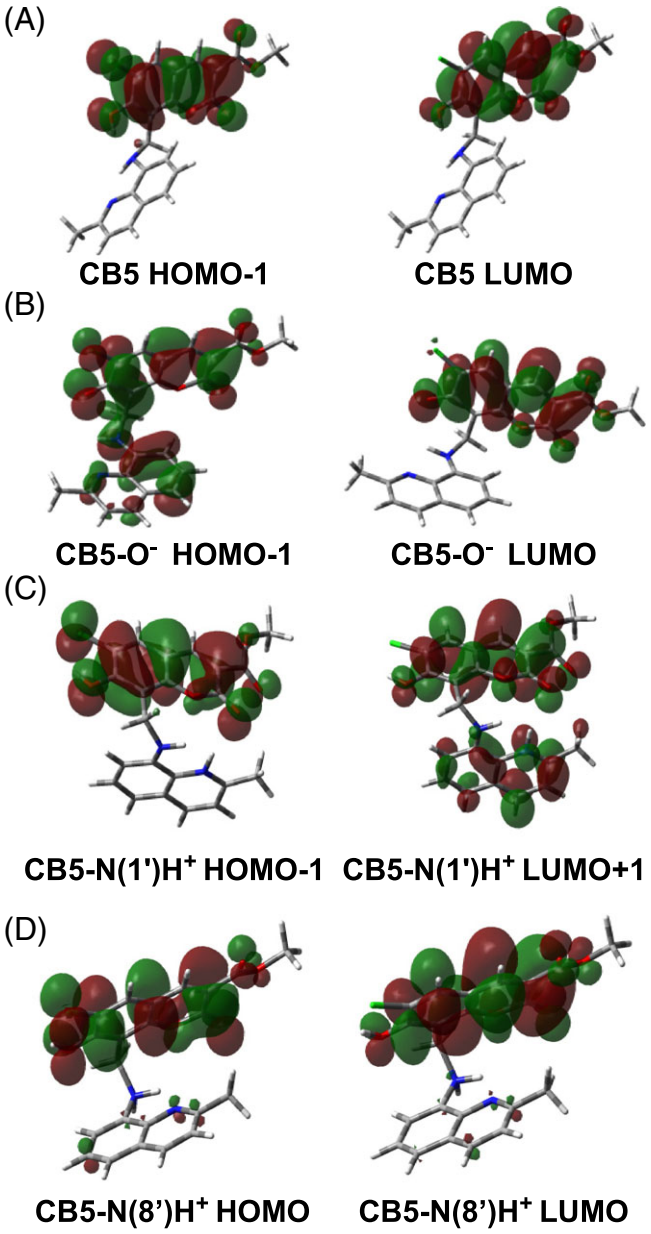

FIGURE 4 Molecular orbital (MO) pairs with dominant contributions to the λ_{max} TD-DFT excitations of A, **CB5**; B, **CB5-O$^-$**; C, **CB5-N(1′)H$^+$**; and D, **CB5-N(8′)H$^+$** displayed with an isovalue of ca. 0.02 e$^-$/Å (TD-CAM-B3LYP/6-311G** level of theory)[36]

delocalized over the entire molecule. Figure 4C shows this exemplary for **CB5-N(1′)H$^+$**, which exhibits a strong absorption with an oscillator strength of f = 0.384 and an excitation energy of 3.90 eV, corresponding to λ_{max} = 318 nm. The calculated spectra shown in Figure 5B reveal that **CB5** and **CB5-N(1′)H$^+$** are virtually indistinguishable in this wavelength region, clearly showing that protonation of the aminoquinoline moiety has no influence on the absorption in the visible region of the electromagnetic spectrum.

Additional geometry optimizations of the relevant excited states of the five protonated/deprotonated **CB5** species revealed little change in the overall relative

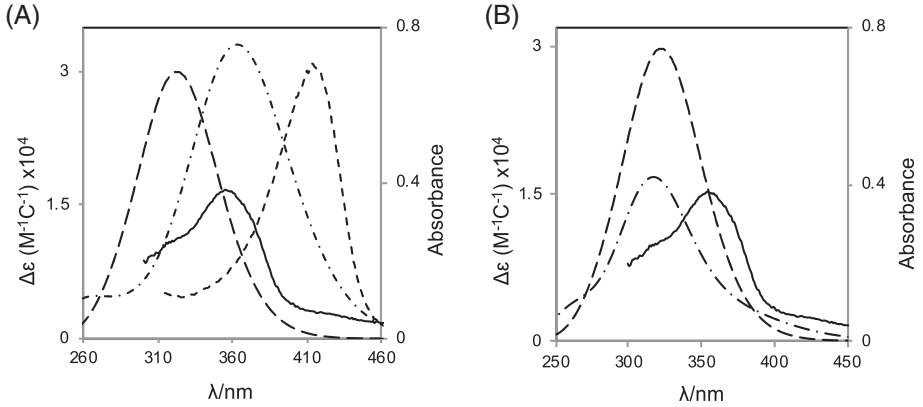

FIGURE 5 A, Simulated UV/vis spectrum (left y-axis) of **CB5** (- - -) and **CB5-O**$^-$ (- • -) vs the experimentally measured absorbance (right y-axis) at pH 1 (——) and pH 7 (- - -). B, Simulated UV/vis spectrum (left y-axis) of **CB5** (- - -) and **CB5-N(1′)H**$^+$ (- • -) vs the experimentally measured absorbance (right y-axis) at pH 1 (——)

arrangement of the two conjugated ring systems compared with the ground-state geometries. The resulting Stokes shifts range from 0.28 eV (34 nm) for **CB5-O**$^-$ to 0.49 eV (44 nm) for **CB5-N(8′)H**$^+$ (see Table S4 for all data). Since the experimental emission spectrum was measured at pH 7, only the computed data for **CB5-O**$^-$ are of relevance. The bright emission for this system is reflected by a large calculated oscillator strength (f = 0.990). The computed emission energy of 400 nm is by 48 nm blue shifted compared with the experiment (see Table 1), however, when converted to eV, this deviation is within the expected error for the chosen method (see Computational Methods). Despite this deviation in the emission energies, we observe nearly perfect agreement between the calculated Stokes shift (0.28 eV or 34 nm) and the experimental value (0.26 eV or 38 nm). This finding again underlines the robustness of our chosen computational approach as well as the validity of the calculated data and their interpretation.

4 | ASSESSMENT OF CB1-5 AS PROBES FOR DETECTING NO•

After having obtained detailed knowledge of the photophysical properties of **CB1-5** in the absence of both Cu(II) and NO•, we next assessed their performance as probes for sensing NO• through replacement of complex bound Cu(II) via an irreversible redox process that is associated with fluorescence turn-on (see Scheme 1). Cu(II)-complexes of **CB1-5**, eg, **Cu(II)-CB1-5**, were prepared by mixing equimolar amounts of $CuCl_2$ with the respective probe. As Figure 6A clearly shows, the fluorescence intensity was quenched upon addition of $CuCl_2$, but the extent to which quenching occurred depended on the conditions. Thus, when DMSO was used as sole solvent (**CB2** was explored as example), reaction of Cu(II) with the probe resulted in almost complete fluorescence quenching. In contrast to this, considerable background fluorescence remained when this reaction was performed in aqueous TBS buffer at pH 7 (with 1% DMSO). Here, the largest drop in fluorescence upon reaction with $CuCl_2$ was found with the most acidic probes **CB4** and **CB5** (44% and 43% respectively), whereas in the case of the considerably less acidic **CB1** and **CB3** systems fluorescence quenching was less efficient (25% and 18%, respectively).

The response of **Cu(II)-CB1-5** to NO• was explored using 6-(2-hydroxy-1-methyl-2-nitrosohydrazino)-*N*-methyl-1-hexanamine (MAHMA NONOate) as a source of NO•.[39] Freshly prepared **Cu(II)-CB1-5** (100 μM in TBS at pH 7 with 1% DMSO) was treated with 400 equivalents of MAHMA NONOate (using stock solutions in NaCl, followed by dilution with TBS at pH 7.6), and fluorescence emission was measured after 30 minutes. As shown in Figure 6B, an increase in fluorescence intensity was observed, ranging from 1.4-fold in the case of **CB1** to 2.7-fold in the case of **CB5**, indicating successful detection of NO•. For **CB2**, the reaction was performed in neat DMSO, which showed a more pronounced increase in fluorescence upon reaction with NO•. The lower background fluorescence of **Cu(II)-CB2** in this solvent and the generally higher fluorescence emission intensity of these probes in DMSO are likely responsible for this effect. Measurements of the fluorescence emission intensity of **Cu(II)-CB5** at different concentrations of the NO• donor revealed that this probe, which is the most emissive in this series at physiological pH, enables detection of [NO•] in μM concentrations (Figure S23).[40] Time-dependent fluorescence emission studies revealed that the reaction of **Cu(II)-CB5** with NO• was complete after about 9 minutes (Figure S24).

The selectivity of the **CB** probes towards NO• was examined by measuring the fluorescence emission of **Cu(II)-CB1-5** upon addition of 400 equivalents of a selection of reactive nitrogen and oxygen species (RNS and ROS), ie, ClO^-, H_2O_2, K_2O_2, NO_3^-, and NO_2^-, which

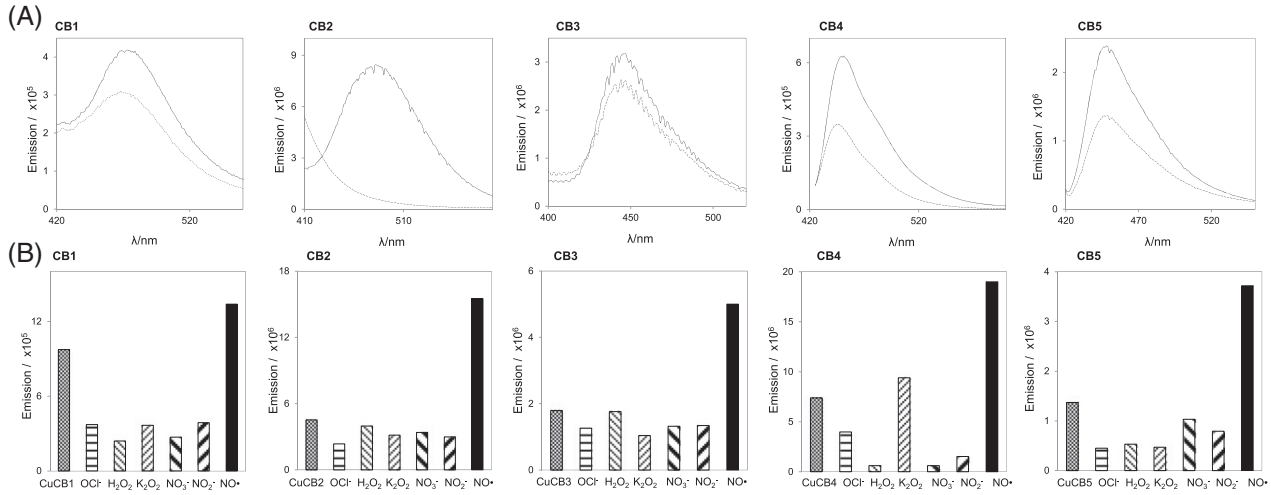

FIGURE 6 A, Fluorescence quenching of **CB1-5** by addition of equimolar amounts of $CuCl_2$ (100 μM in TBS at pH 7 with 1% DMSO) **CB1-5** (solid line) and **Cu(II)-CB1-5** (dotted line). B, Selectivity of **Cu(II)-CB1-5** towards NO• and a series of RNS and ROS (100 μM in TBS at pH 7 with 1% DMSO; 400 equiv. of oxidant). The reactions with **CB2** in (A) and (B) were performed in neat DMSO

have been typically used to assess probe selectivity for NO•.[41] The data in Figure 6B clearly show that none of these ROS and RNS led to a fluorescence increase, which is similar to the sensors developed by Lippard et al.[17,18] In most cases, the fluorescence dropped, except for the reaction of **Cu(II)-CB4** with K_2O_2, where a slight increase (21%) was observed. However, this fluorescence increase was significantly less than the increase observed for the reaction of **Cu(II)-CB4** with NO• (61%), which demonstrates the generally high selectivity of all **CB** probes studied here for NO•.

5 | NO• DETECTION IN BIOLOGICAL SYSTEMS

Finally, preliminary fluorescence imaging studies were performed to obtain a qualitative assessment of the capacity of the probes to detect NO•in living bacterial cells. For this, we compared the two most emissive probes, eg, the previously reported **CB5**,[42] and **CB4**, using 24-hour-old biofilms of *Pseudomonas aeruginosa* as the model organism, by employing a protocol previously devised by one of us (see Experimental Section).[41] Briefly, NO• production was stimulated by treating the cells with a 10 mM aqueous solution of KNO_3, which is reduced to produce NO• in mM concentrations.[43,44] After 3 hours, these cells were treated with freshly prepared Cu complexes of the probes and incubated for 1 hour at 37°C. To demonstrate the performance of the probes in multi-dye imaging experiments, the cells were also treated with HCS (NuclearMask Deep Red stain), which stains DNA in both living and dead cells. The cells were subsequently examined at 37°C using confocal laser-scanning microscopy. Representative cell images are presented in Figure 7 for **CB4** (top) and **CB5** (bottom). Blue fluorescence, which is due to reaction of **Cu(II)-CB4** or **Cu(II)-CB5** with endogenously produced NO•, is clearly visible in Figure 7A,D. It should be noted that previous studies with **Cu(II)-CB5** in macrophages confirmed that other constituents of the cytoplasm, for example glutathione, did not lead to a fluorescence turn-on.[20,45]

The overlaid images in Figure 7C,F demonstrate convincingly that **CB4** and **CB5** are both cell permeable and that the blue fluorescing cells can be easily distinguished from the HCS stained red fluorescing cells (Figure 7B,E, respectively). Finally, qualitative comparison of the fluorescence intensities in these images reveals that **CB5** is much brighter than **CB4**. This finding is in excellent agreement with the results of the fluorescence emission studies shown in Figure 1, clearly confirming the importance of a fully deprotonated coumarin moiety at physiological pH to achieve the highest sensitivity for NO• detection in bacterial cell systems.

6 | CONCLUSIONS

We have synthesised the coumarin-based probes **CB1-5** and investigated their photophysical properties to provide guidelines for the design of blue fluorescence "turn-on" sensors for the detection of endogenously produced NO• using the replacement strategy. Electron-withdrawing ester groups at C-3 of the coumarin moiety (as in **CB3**, **CB4**, and **CB5**) lead not only to blue fluorescence emission at $\lambda \sim 450$ nm but also enable excitation at $\lambda = 405$ nm that is suitable for confocal laser scanning microscopy studies in multi-dye imaging experiments. Experiments and TD-DFT calculations revealed that the observed fluorescence is due

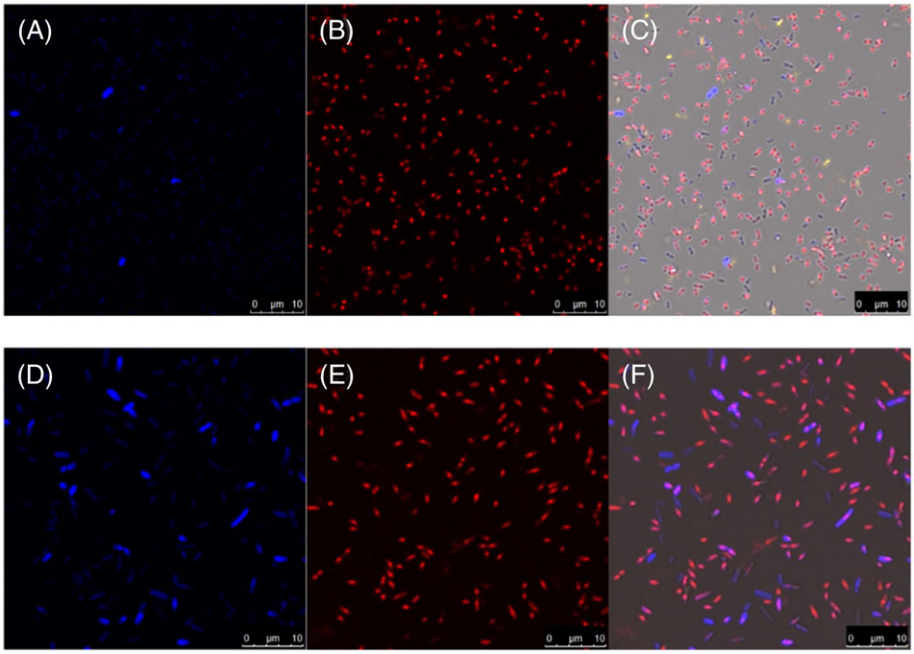

FIGURE 7 NO• detection in 24-h *P. aeruginosa* biofilms that were up-regulated for NO• production using confocal laser-scanning microscopy. NO• detected with **CB4** A, and **CB5** D, HCS stained live and dead cells in the presence of **CB4** B, and **CB5** E, overlaid images of **CB4** and HCS C, and **CB5** and HCS F

to the *O*-deprotonated coumarin moiety, whereas the "neutral" probes exhibit only a weak fluorescence intensity. These findings clearly show that coumarin-based probes must be fully deprotonated at physiological pH to ensure a high sensitivity for NO• in biological systems. This deprotonation can be achieved by electron-withdrawing substituents at C-6 on the coumarin moiety (*ortho* to the hydroxyl group), for example chlorine, as in **CB5**. Generally, all of the probes **CB1-5** enabled selective detection of NO• without interference by a variety of ROS and RNS. Preliminary fluorescence imaging studies demonstrated that both **CB4** and **CB5**, which are the most acidic and therefore most emissive probes studied in this work, can be successfully used to detect NO• in living *P. aeruginosa* cells. Future work is aimed at improving the complexation properties of the probes to reduce the background fluorescence of the Cu(II) complexes, while maintaining or even further increasing the acidity of the OH group on the coumarin moiety to enhance their sensitivity for detecting NO• beyond the μM concentration range.

EXPERIMENTAL SECTION

1. Synthetic Materials and Methods

Unless otherwise noted, reagents were obtained from commercial suppliers and were used without further purification. All anhydrous reactions were performed in oven-dried or flame-dried glassware under argon. NMR spectra were recorded on an Agilent NMR400, Agilent DD2 or Bruker Advance IIIHD instrument. Chemical shifts (δ) are reported in parts per million (ppm). High-resolution mass spectroscopy (HRMS) was conducted on a Finnigan hybrid linear triple-quadrupole (LTQ) Fourier transform ion cyclotron resonance (FTICR) mass spectrometer. Reverse phase preparative HPLC was performed on an Agilent 1200 series HPLC system with a Phenomenex Luna C18(2) 100A packed (50 mm × 21.2 mm × 5 μm) Axia column. Compound purity was assessed by analytical reverse phase HPLC on an Agilent 1100 series HPLC system with a Phenomenex Aeris peptide XB-C18 packed (250 mm × 4.6 mm × 3.6 μm) column. 7-Hydroxy-4-methylcoumarin **1b** was purchased from Sigma Aldrich and directly used. The 7-hydroxycoumarins **1a**, **1c**, and **1d** were prepared according to literature.[22] Synthesis of the formylated coumarins **2a** and **2b** was performed as described in Huang et al.[23] The NMR spectra and HPLC traces for **CB1-4** are given in the ESI. **CB5** was obtained as described in Barzegar Amiri Olia et al. [20]

a. **Ethyl 7-hydroxy-8-formyl-coumarin-3-carboxylate (2c).** A solution of **1c** (1 g, 4.27 mmol) and hexamine (898 mg, 6.4 mmol) in trifluoroacetic acid (9 mL) was heated under reflux for 20 hours, and then 18-mL water was added. The solution was further stirred for 30 minutes at 60°C. After cooling,

the precipitate was collected by filtration to give **2c** as yellow solid (60%). ^{1}H NMR (400 MHz, $CDCl_3$): δ 10.38 (s, 1H), 8.72 (s, 1H), 8.02 (d, ^3J = 8 Hz, 1H), 6.98 (d, ^3J = 8.8 Hz, 1H), 4.25 (q, ^3J = 7.2 Hz, 2H), 1.27 ppm (t, ^3J = 7.2 Hz, 3H).

b. **Methyl 7-hydroxy-8-formyl-coumarin-3-carboxylate (2d).** A solution of **1d** (1 g, 4.54 mmol) and hexamine (956 mg, 6.82 mmol) in trifluoroacetic acid (9 mL) was heated under reflux for 20 hours, and then 60-mL water was added. The mixture was stirred for a further 30 minutes at 60°C. After cooling, the precipitate was collected by filtration to give **2d** as a yellow solid (53%). ^{1}H NMR (500 MHz, $CDCl_3$): δ 12.53 (s, 1H), 10.61 (s, 1H), 8.56 (s, 1H), 7.73 (d, ^3J = 8.8 Hz, 1H), 6.96 (d, ^3J = 8.8 Hz, 1H), 3.97 ppm (s, 1H).

c. **CB1.** To a stirred solution of **2a** (210 mg, 0.79 mmol) in anhydrous methanol (32 mL) at room temperature was added 2-methyl-8-aminoquinoline (125 mg, 0.79 mmol). The mixture was stirred at room temperature for 8 hours under argon. The solution was cooled to 0°C, sodium borohydride (230 mg, 6 mmol) was added, and the reaction mixture was stirred overnight at room temperature. The solvent was evaporated in vacuo, and the crude material purified by column chromatography (SiO_2, ethyl acetate/petroleum spirits 1:1) to give **CB1** as a yellow solid (80%). ^{1}H NMR (500 MHz, DMSO-d_6): δ 8.15 (s, 1H), 8.06 (d, ^3J = 10.5 Hz, 1H), 7.70-7.68 (m, 2H), 7.54 (d, ^3J = 11 Hz, 1H), 7.45-7.41 (m, 2H), 7.37 (d, ^3J = 9.5 Hz, 1H), 7.33 (d, ^3J = 10.5 Hz, 1H), 7.28 (t, ^3J = 9.5 Hz, 1H), 7.01 (d, ^3J = 10.5 Hz, 1H), 6.97 (d, ^3J = 9.5 Hz, 1H), 6.91 (d, ^3J = 10.5 Hz, 1H), 6.54 (t, ^3J = 7 Hz, NH), 4.6 (d, ^3J = 6.5 Hz, 2H), 2.56 ppm (s, 3H). ^{13}C NMR (125 MHz, DMSO-d_6): δ 160.35, 155.79, 153.62, 143.99, 143.98, 137.35, 136.63, 135.45, 129.27, 128.70, 128.65, 128.48, 127.11, 126.71, 122.74, 114.09, 113.38, 112.49, 112.41, 106.33, 35.62, 25.25 ppm. HRMS (ESI$^+$); calcd. for $C_{26}H_{21}N_2O_3^+$ 409.15467 $[M + H]^+$, found 409.15422.

d. **CB2.** To a stirred solution of **2b** (80 mg, 0.39 mmol) in dry methanol (16 mL) at room temperature was added 2-methyl-8-aminoquinoline (68 mg, 0.43 mmol). The mixture was stirred at room temperature for 8 hours under argon. The solution was cooled to 0°C, sodium borohydride (114.2 mg, 3 mmol) was added, and the reaction mixture was stirred overnight at room temperature. The solvent was evaporated in vacuo and the crude material purified by column chromatography (SiO_2, ethyl acetate/petroleum spirits 2:3) to give **CB2** as a yellow solid (51%). ^{1}H NMR (500 MHz, DMSO-d_6): δ 10.88 (s, 1H), 8.06 (d, ^3J = 8.5 Hz, 1H), 7.54 (d, ^3J = 8.5 Hz, 1H), 7.33 (d, ^3J = 8 Hz, 1H), 7.27 (t, ^3J = 8 HZ, 1H), 7.01 (d, ^3J = 7.5 Hz, 1H), 6.95 (d, ^3J = 7 Hz, 1H), 6.90 (d, ^3J = 9 Hz, 1H), 6.54 (NH, 1H), 6.15 (s, 1H), 4.58 (s, 2H), 2.57 (s, 3H), 2.34 ppm (s, 3H); ^{13}C NMR (125 MHz, DMSO-d_6): δ 160.46, 159.91, 155.78, 154.34, 153.5, 143.91, 137.24, 136.71, 127.10, 126.71, 125.80, 122.72, 114.09, 112.73, 112.69, 112.55, 110.57, 106.41, 35.69, 25.18, 18.69 ppm. HRMS (ESI$^+$); calcd. for $C_{21}H_{19}N_2O_3^+$ 347.13902 $[M + H]^+$, found 347.13855.

e. **CB3.** To a stirred solution of **2c** (100 mg, 0.38 mmol) in dry dichloromethane (30 mL) at room temperature was added a solution of 2-methyl-8-aminoquinoline (67 mg, 0.42 mmol) in dry methanol (20 mL) and activated MS (4 Å). The mixture was stirred at room temperature for 8 hours under argon. The solution was cooled to 0°C, sodium triacetoxy borohydride (161 mg, 0.76 mmol) was added, and the reaction mixture was stirred overnight at room temperature. The solvent was evaporated in vacuo and the crude material purified by column chromatography (SiO_2, ethyl acetate/petroleum spirits 3:2) to give **CB3** as a yellow solid (70%). ^{1}H NMR (500 MHz, $CDCl_3$): δ 8.65 (s, 1H), 8.05 (d, ^3J = 8.5 Hz, 1H), 7.69 (d, ^3J = 9 Hz, 1H), 7.33 (d, ^3J = 8.5 Hz, 1H), 7.27 (t, ^3J = 7.5 Hz, 1H), 7.01 (d, ^3J = 7.5 Hz, 1H), 6.93 (d, ^3J = 7.5 Hz, 1H), 6.55 (NH, 1H), 4.57 (s, 2H), 4.25 (q, ^3J = 7 Hz, 1H), 2.58 (s, 3H), 1.28 ppm (t, ^3J = 7.5 Hz, 3H). ^{13}C NMR (125 MHz, $CDCl_3$): δ 163.31, 162.90, 156.68, 155.81, 155.64, 150.25, 143.89, 137.34, 136.62, 131.38, 127.07, 126.7, 122.74, 114.16, 113.87, 112.57, 112.27, 110.92, 106.29, 61.28, 35.48, 25.25, 14.59 ppm. HRMS (ESI$^+$); calcd. for $C_{23}H_{21}N_2O_5^+$ 405.14450 $[M + H]^+$, found 405.14398.

f. **CB4.** To a stirred solution of **2d** (100 mg, 0.4 mmol) in dry dichloromethane (30 mL) at room temperature was added a solution of 2-methyl-8-aminoquinoline (60 mg, 0.4 mmol) in dry methanol (20 mL) and activated MS (4 Å). The mixture was stirred at room temperature for 8 hours under argon. The solution was cooled to 0°C, sodium triacetoxy borohydride (109 mg, 0.8 mmol) was added, and the reaction mixture was stirred overnight at room temperature. The crude material was purified by column chromatography (SiO_2, ethyl acetate/petroleum spirits 3:2) to give **CB4** as a yellow solid (64%). ^{1}H NMR (500 MHz, $CDCl_3$): δ 8.66 (s, 1H), 8.04 (d, J = 8.5 Hz, 1H), 7.67 (d, ^3J = 8.5 Hz, 1H), 7.32 (d, ^3J = 8.5 Hz, 1H), 7.27 (t, ^3J = 8 Hz, 1H), 7.01 (d, ^3J = 8 Hz, 1H), 6.94-6.92(m, 2H), 6.53 (NH, 1H), 4.56 (s, 2H), 3.78 (s, 3H), 2.58 ppm (s, 3H). ^{13}C NMR (125 MHz, $CDCl_3$): δ 163.87, 163.01, 156.65, 155.81, 155.68, 150.58, 143.87, 137.33, 136.61, 131.42 127.06, 126.69, 122.74, 114.17, 113.86, 112.56, 111.94, 110.93, 106.29,

52.58, 35.46, 25.23 ppm. HRMS (ESI^+); calcd. For $C_{22}H_{19}N_2O_5^+$ 391.12885 $[M + H]^+$, found 391.12844.

2. Photophysical studies

UV/vis absorption spectra were recorded using an Agilent 8453 UV/vis absorbance spectrophotometer. Fluorescence spectroscopy was conducted on a Horiba Jobin Yvon Fluorolog-3. Tris (hydroxymethyl) aminomethane (Tris) (99.8%, Sigma Aldrich) and sodium chloride were utilised to prepare buffered TBS solutions (50 mM Tris and 150 mM NaCl) in Milli-Q H_2O and the pH adjusted to 7.6 with 1.0 M HCl. MAHMA NONOate ($NO^{\bullet}$donor) was purchased from Sigma Aldrich and stored in the fridge until used. MAHMA NONOate was prepared as stock solution (1 mM in aqueous NaCl) and diluted with TBS to the required concentrations. Stock solutions of the individual RNS and ROS were prepared in aqueous media (1 mM in Milli-Q H_2O). $CuCl_2{\cdot}2H_2O$ was used to prepare 1 mM $CuCl_2$ stock solutions in Milli-Q H_2O. Stock solutions of **CB1-5** were freshly prepared in DMSO (1 mM) prior to the experiments and then diluted with TBS as required. **Cu(II)-CB1-5** solutions ($CuCl_2$/**CB1-5** 1:1) were prepared immediately prior to the experiments. The solutions for the selectivity measurements were prepared by addition of the RNS and ROS stock solutions into the **Cu(II)-CB1-5** solution.

3. Computational methods (see also SI)

Initial sampling of the conformational space of five different forms of the **CB4** and **CB5** was accomplished with the MMX force-field as implemented in PCMODEL 9.3.[46] Subsequent geometry optimizations were performed at the dispersion-corrected DFT level with the TPSS[47] density functional approximation (DFA), Grimme's DFT-D3 dispersion correction with Becke-Johnson damping[48] and the def2-TZVP[49] triple-ζ Ahlrichs AO basis set (TPSS-D3/def2-TZVP). This level of theory was shown to deliver accurate geometries of larger molecular systems at low computational cost, while additionally having an advantage over the commonly chosen approaches, such as B3LYP/6-31G* or BP86/6-31G*, by taking into account ubiquitous London-dispersion effects and avoiding artefacts due to basis-set incompleteness errors.[48,50] Subsequently, single-point calculations at the dispersion-corrected double-hybrid[51] level (PWPB95[52]-D3/def2-TZVPP) were carried out to obtain the relative energies between the various conformers. This DFA has been proven to be one of the most accurate DFT methods for the determination of these types of energies and the calculation of proton affinities (PA).[53] All these calculations were carried out with the ORCA 3.0.3 software package with ORCA's numerical quadrature grid "5" and the resolution-of-the-identity approximation to speed up the evaluation of Coulomb integrals and the second-order perturbative correlation portion of the PWPB95 double hybrid.[54] The resulting relative energies and the Cartesian coordinates of all optimised conformers are provided in the Supporting Information. TD-DFT calculations were carried out with Gaussian09 Revision B.01.[55] Since the existence of charge-transfer (CT) excitations could not be ruled out, the range-separated hybrid DFA CAM-B3LYP[31] was employed, which has been shown to be reliable for the calculation of vertical singlet-singlet excitation energies in medium-sized organic dyes with an average absolute error of about 0.18 eV and an expected average overestimation of the excitation energies by 0.11 eV.[33] As outlined in the SI, preliminary tests with an alternative functional approximation gave the same insights, thus, demonstrating the reliability of our chosen approach. The 6-311G**[32] Pople-type triple-ζ AO basis set and the standard Gaussian quadrature integration grid were used for all calculations. The first seven excitation energies were calculated together with their oscillator strengths (f). When required, solvent effects were simulated with Gaussian's default polarizable continuum solvation model (PCM)[56] and appropriate dielectric constants and refractive indices for the solvents of interest. The UV/vis absorption spectra were simulated by the standard technique of overlapping Gaussian functions for each transition with a value of 0.4 eV for the half-width of the absorption band at a height of 1/e. Excited-state geometry optimizations of the first bright state in each system of the **CB5**-type were also carried out at the TD-CAM-B3LYP/6-311G** level of theory.

4. Confocal microscopy imaging studies

Overnight cultures of *P. aeruginosa* were diluted by 100 times in buffered peptone water medium and inoculated in a μ-slide 8-well microscopy chamber (Ibidi, 100 μL per well). The chamber was incubated for 24 hours at ambient temperatures (19°C-22°C). Then the media was replaced with freshly prepared 10 mM solution of buffered peptone water-KNO_3 and incubated for 3 hours at ambient temperatures (19°C-22°C). The resultant biofilms within the wells were treated with the probes and HCS stains.[42] The probes (**CB4** and **CB5**) were freshly prepared prior to the experiments as 1 mM stock solutions in DMSO and diluted to 10 μM with TBS for cell staining. HCS NuclearMaskTM Deep Red stain (HCS) was purchased from Thermo Fisher Scientific as a X1000 concentrate in DMSO and stored in the freezer under exclusion of direct light until used. HCS was

diluted by a factor of 500 in TBS before use. The resultant biofilms within the wells were first treated with potassium nitrate to induce NO• production. After 3 hours of incubation at 37°C, the wells were treated with freshly prepared **Cu(II)-CB4,5** (10 μM in TBS with 1% DMSO) for 1 hour in the dark, rinsed with TBS (2 × 100 μL) and stained with HCS for 30 minutes in the dark. **CB4,5-NO** and HCS were visualised with a Leica SP5 Inverted Laser Scanning Microscope using a 405 laser (λ = 405 nm) and Helium-Neon laser (λ = 633 nm), respectively. Images were collected with Leica LAS AF software and formatted with ImageJ.

ACKNOWLEDGEMENTS

This work was supported by the University of Melbourne, the Australian Research Council through the Australian Discovery Early Career Researcher Award Scheme (L.G., DE140100550), the Centres of Excellence Scheme (CE0561607) and the Discovery Scheme (DP13010007), the National Computational Infrastructure (NCI) National Facility, the Victorian Life Sciences Computation Initiative (VLSCI, now Melbourne Bioinformatics), and the High Performance Computing Facility of the University of Melbourne. We thank Paul McMillan at the Biological Optical Microscopy Platform (BOMP, University of Melbourne) for the confocal microscopy images.

ORCID

Lars Goerigk http://orcid.org/0000-0003-3155-675X
Uta Wille http://orcid.org/0000-0003-1756-5449

REFERENCES

[1] J. W. Coleman, *Intern. Immunopharm.* **2001**, *1*, 1397.

[2] J. O. Lundberg, M. T. Gladwin, E. Weitzberg, *Nat. Rev. Drug Discov.* **2015**, *14*, 623.

[3] a) N. Barraud, D. J. Hassett, S.-H. Hwang, S. A. Rice, S. Kjelleberg, J. S. Webb, *J. Bacteriol.* **2006**, *188*, 7344. b) N. Barraud, D. Schleheck, J. Klebensberger, J. S. Webb, D. J. Hassett, S. A. Rice, S. Kjelleberg, *J. Bacteriol.* **2009**, *191*, 7333. c) N. Liu, Y. Xu, S. Hossain, N. Huang, D. Coursolle, J. A. Gralnick, E. M. Boon, *Biochemistry* **2012**, *51*, 2087. d) D. McDougald, S. A. Rice, N. Barraud, P. D. Steinberg, S. Kjelleberg, *Nat. Rev. Microbiol.* **2012**, *10*, 39.

[4] a) T. R. Bott, *Appl. Therm. Eng.* **1998**, *18*, 1059. b) F. Y. Chye, A. Abdullah, M. K. Ayob, *Food Microbiol.* **2004**, *21*, 535. c) J. Klahre, H. C. Flemming, *Water Res.* **2000**, *34*, 3657. d) M. Nemati, G. E. Jenneman, G. Voordouw, *Biotechnol. Bioeng.* **2001**, *74*, 424.

[5] D. Lindsay, A. von Holy, *J. Hosp. Infect.* **2006**, *64*, 313.

[6] O. Ciferri, *Appl. Environ. Microbiol.* **1999**, *65*, 879.

[7] a) J. W. Costerton, P. S. Stewart, E. P. Greenberg, *Science* **1999**, *284*, 1318. b) W. A. Smith, *Adv. Drug Deliv. Rev.* **2005**, *57*, 1539.

[8] P. K. Singh, A. L. Schaefer, M. R. Parsek, T. O. Moninger, M. J. Welsh, E. P. Greenberg, *Nature* **2000**, *407*, 762.

[9] N. Cerca, S. Martins, F. Cerca, K. K. Jefferson, G. B. Pier, R. Oliveira, J. Azeredo, *J. Antimicrob. Chemother.* **2005**, *56*, 331.

[10] J. D. Bryers, *Biotechnol. Bioeng.* **2008**, *100*, 1.

[11] a) I. Banerjee, R. C. Pangule, R. S. Kane, *Adv. Mater.* **2011**, *23*, 690. b) K. Bazaka, M. V. Jacob, R. J. Crawford, E. P. Ivanova, *Appl. Microbiol. Biotechnol.* **2012**, *95*, 299. c) M. Kargar, A. Pruden, W. A. Ducker, *J. Mater. Chem. B* **2014**, *2*, 5962.

[12] a) M. Gjermansen, M. Nilsson, L. Yang, T. Tolker-Nielsen, *Mol. Microbiol.* **2010**, *75*, 815. b) S. M. Hunt, E. M. Werner, B. Huang, M. A. Hamilton, P. S. Stewart, *Appl. Environ. Microbiol.* **2004**, *70*, 7418.

[13] N. R. Yepuri, N. Barraud, N. S. Mohammadi, B. G. Kardak, S. Kjelleberg, S. A. Rice, M. J. Kelso, *Chem. Commun.* **2013**, *49*, 4791.

[14] Selected examples a) L. Wang, P. Hu, X. Deng, F. Wang, Z. Chen, *Biosens. Bioelectron.* **2013**, *50*, 57. b) P. Yáñez-Sedeño, L. Agüí, J. M. Pingarrón, Carbon nanotubes-based microelectrode (bio)sensors, in *Microelectrode Biosensors*, (Eds: S. Marinesco, N. Dale) Vol. 80, Neuromethods; Humana Press, Totowa, NJ **2013** 281. c) N. J. Finnerty, S. L. O'Riordan, E. Palsson, J. P. Lowry, J. Neurosci, *Methods* **2012**, *209*, 13. d) R. A. Hunter, B. J. Privett, W. H. Henley, E. R. Breed, Z. Liang, R. Mittal, B. P. Yoseph, J. E. McDunn, E. M. Burd, C. M. Coopersmith, J. M. Ramsey, M. H. Schoenfisch, *Anal. Chem.* **2013**, *85*, 6066. e) H. Asakawa, S. Ikeno, T. Haruyama, *Sens. Actuators B* **2005**, *108*, 646.

[15] Selected examples a) H. Kojima, M. Hirotani, N. Nakatsubo, K. Kikuchi, Y. Urano, T. Higuchi, Y. Hirata, T. Nagano, *Anal. Chem.* **2001**, *73*, 1967. b) N. Nakatsubo, H. Kojima, K. Sakurai, K. Kikuchi, H. Nagoshi, Y. Hirata, T. Akaike, Y. Urano, T. Higuchi, T. Nagano, *Biol. Pharm. Bull.* **1998**, *21*, 1247. c) H. Kojima, N. Nakagtsubo, K. Kiguchi, Y. Urano, T. Higuchi, J. Tanaka, Y. Kudo, T. Nagano, *Neuropharmacology* **1998**, *9*, 3345. d) N. M. Iverson, P. W. Barone, M. Shandell, L. J. Trudel, S. Sen, F. Sen, V. Ivarov, E. Atolia, E. Farias, T. P. McNicholas, N. Reuel, N. M. A. Parry, G. N. Wogan, M. S. Strano, *Nat. Nanotech.* **2013**, *8*, 873. e) M. H. Lim, S. J. Lippard, *Acc. Chem. Res.* **2007**, *40*, 40. f) R. C. Smith, A. G. Tennyson, A. C. Won, S. J. Lippard, *Inorg. Chem.* **2006**, *45*, 9367. g) R. C. Smith, A. G. Tennyson, A. C. Won, S. J. Lippard, *Org. Lett.* **2005**, *7*, 3573.

[16] Selected examples a) M. Barzegar Amiri Olia, C. H. Schiesser, M. K. Taylor, *Org. Biomol. Chem.* **2014**, *12*, 6757. b) H. Yu, X. Zhang, Y. Xiao, W. Zou, L. Wang, L. Jin, *Anal. Chem.* **2013**, *85*, 7076. c) X. Hu, J. Wang, X. Zhu, D. Dong, X. Zhang, S. Wu, C. Duan, *Chem. Commun.* **2011**, *47*, 11507. d) H. Yu, L. Jin, Y. Dai, H. Li, Y. Xiao, *New J. Chem.* **2013**, *37*, 1688. e) J.-B. Chen, H.-X. Zhang, X.-F. Guo, H. Wang, H.-S. Zhang, *Anal. Chim. Acta* **2013**, *800*, 77. f) C. Sun, W. Shi, Y. Song, W. Chen, H. Ma, *Chem. Commun.* **2011**, *47*, 8638. g) R. Zhang, Z. Ye, G. Wang, W. Zhang, J. Yuan, *Chem. A Eur. J.* **2010**, *16*, 6884. h) C. Yu, Y. Wu, F. Zeng, S. Wu, *J. Mater. Chem. B* **2013**, *1*, 4152.

[17] a) U.-P. Apfel, D. Buccella, J. J. Wilson, S. J. Lippard, *Inorg. Chem.* **2013**, *52*, 3285. b) G. K. Vegesna, S. R. Sripathi, J. Zhang,

S. Zhu, W. He, F.-T. Luo, W. J. Jahng, M. Frost, H. Liu, *ACS Appl. Mater. Interfaces* **2013**, *5*, 4107. c) W.-T. Shiue, Y.-H. Chen, C.-M. Wu, G. Singh, H.-Y. Chen, C.-H. Hung, W.-F. Liaw, Y.-M. Wang, *Inorg. Chem.* **2012**, *51*, 5400.

[18] a) M. H. Lim, S. J. Lippard, *Acc. Chem. Res.* **2006**, *40*, 41. b) M. H. Lim, S. J. Lippard, *Inorg. Chem.* **2006**, *45*, 8980. c) M. H. Lim, B. A. Wong, W. H. Pitcock, D. Mokshagundam, M.-H. Baik, S. J. Lippard, *J. Am. Chem. Soc.* **2006**, *128*, 14364. d) L. E. McQuade, S. J. Lippard, *Inorg. Chem.* **2010**, *49*, 7464. e) S. C. Bourdette, G. K. Walkup, B. Spingler, R. Y. Tsien, S. J. Lippard, *J. Am. Chem. Soc.* **2001**, *123*, 7831. f) M. D. Pluth, M. R. Chan, L. E. McQuade, S. J. Lippard, *Inorg. Chem.* **2011**, *50*, 9385.

[19] V. C. Ezeh, T. C. Harrop, *Inorg. Chem.* **2013**, *52*, 2323.

[20] a) M. Barzegar Amiri Olia, A. Zavras, C. H. Schiesser, S.-A. Alexander, *Org. Biomol. Chem.* **2016**, *14*, 2272. b) M. M. Sadek, M. Barzegar Amiri Olia, C. J. Nowell, N. Barlow, C. H. Schiesser, S. E. Nicholson, R. S. Norton, *Bioorg. Med. Chem.* **2017**, *25*, 5743.

[21] The detailed mechanism of the fluorescence quenching in the Cu(II) complexes is not clear. For recent reviews of fluorescence quenching and sensing mechanisms see a) D. Escudero, *Acc. Chem. Res.* **2016**, *49*, 1816. b) G.-Y. Li, K.-L. Han, *Wiley Interdiscip. Rev. Comput. Mol. Sci.* **2018**, *8*, e1351.

[22] a) D. Olmedo, R. Sancho, L. M. Bedoya, J. L. Lopez-Perez, E. del Olmo, E. Munoz, J. Alcami, M. P. Gupta, A. San Feliciano, *Molecules* **2012**, *17*, 9245. b) M. D. Mertens, S. Hinz, C. E. Müller, M. Gütschow, *Bioorg. Med. Chem.* **2014**, *22*, 1916.

[23] a) X. Huang, Y. Dong, Q. Huang, Y. Cheng, *Tetrahedron Lett.* **2013**, *54*, 3822. b) L. Long, L. Zhou, L. Wang, S. Meng, A. Gong, F. Du, C. Zhang, *Org. Biomol. Chem.* **2013**, *11*, 8214.

[24] The exposure time during the confocal microscopy studies (ca. 1 min) is too short to cause damage to cell H.-Y. Youn, R. Chou, A. P. Cullen, J. G. Sivak, *J. Photochem. Photobiol. B.* **2009**, *95*, 64. This was confirmed in NO• imaging studies in macrophages using the **CB5** probe; see ref. [20b].

[25] M. Lee, N. G. Gubernator, D. Sulzer, D. Sames, *J. Am. Chem. Soc.* **2010**, *132*, 8828.

[26] S. Protti, A. Mezzetti, *J. Mol. Liq.* **2015**, *205*, 110.

[27] P. Bourbon, Q. Peng, C. Ferraudi, C. Stauffacher, O. Wiest, P. Helquist, *J. Org. Chem.* **2012**, *77*, 2756.

[28] D. L. Gerrard, M. W. Maddams, *Spectrochim. Acta A* **1978**, *34*, 1117.

[29] a) A. E. Lanterna, M. González-Béjac, M. Frenette, J. S. Scaiano, *Photochem. Photobiol. Sci.* **2017**, *16*, 1284. b) J. Seixas de Melo, P. F. Fernandes, *J. Mol. Struct.* **2001**, *565-566*, 69.

[30] a) J. Küpper, M. Schmitt, K. Kleinermanns, *Phys. Chem. Chem. Phys.* **2002**, *4*, 4634. b) V. K. Lacey, A. R. Parrish, S. Han, Z. Shen, S. P. Briggs, Y. Ma, L. Wang, *Angew. Chem. Int. Ed.* **2011**, *50*, 8692.

[31] T. Yanai, D. P. Tew, N. C. Handy, *Chem. Phys. Lett.* **2004**, *393*, 51.

[32] A. D. McLean, G. S. Chandler, *J. Chem. Phys.* **1980**, *72*, 5639.

[33] L. Goerigk, S. Grimme, *J. Chem. Phys.* **2010**, *132*, 184103.

[34] R. K. Bansal, *Heterocyclic Chemistry*, 3rd ed., New Age International (P), Ltd. **1999**.

[35] L. W. Deady, W. L. Finlayson, *Aust. J. Chem.* **1984**, *37*, 1625.

[36] R. Dennington, T. A. Keith, J. M. Millam, *GaussView, Version 5*, Semichem Inc., Shawnee Mission, KS **2009**.

[37] L. Goerigk, J. Moellmann, S. Grimme, *Phys. Chem. Chem. Phys.* **2009**, *11*, 4611.

[38] It should be noted, that, unlike the more popular TD-B3LYP method, TD-CAM-B3LYP has the advantage to being free of artefacts (i.e., ghost states) and does not rely on uncontrollable error compensation; see refs. [33], [37] and SI.

[39] M. Seccia, C. Perugini, E. Albano, G. Bellomo, *Biochem. Biophys. Res. Commun.* **1996**, *220*, 306.

[40] We determined the fluorescence quantum yield, Φ_F, for the **CB5** system (in TBS at pH 7 with 1% DMSO, λ_{ex} = 415 nm, using coumarin 519 as reference). **CB5**: Φ_F = 3.0 %, **Cu(II)-CB5**: Φ_F = 2.6 %, **Cu(II)-CB5** + NO•: Φ_F =12.3 %.

[41] a) L. Yuan, W. Lin, Y. Xie, B. Chen, S. Zhu, *J. Am. Chem. Soc.* **2012**, *134*, 1305. b) C. Yu, Y. Wu, F. Zeng, S. Wu, *J. Mater. Chem. B* **2013**, *1*, 4152. c) R. Miao, L. Mu, H. Zhang, H. Xu, G. She, P. Wang, W. Shi, *J. Mater. Chem.* **2012**, *22*, 3348. d) L. Tan, A. Wan, H. Li, *Analyst* **2013**, *138*, 879. e) G. K. Vegesna, S. R. Sripathi, J. Zhang, S. Zhu, W. He, F.-T. Luo, W. J. Jahng, M. Frost, H. Liu, *ACS Appl. Mater. Interfaces* **2013**, *5*, 4107.

[42] S.-A. Alexander, E. M. Rouse, J. M. White, N. Tse, C. Kyi, C. H. Schiesser, *Chem. Commun.* **2015**, *51*, 3355. see also ref. [3a].

[43] Nanomolar concentrations of NO• are typically present in healthy bacterial cells, where it is produced through denitrifying and nitrifying microorganisms; see also P. G. Wang, T. B. Cai, N. Taniguchi (Eds), *Nitric Oxide Donors: For Pharmaceutical and Biological Applications*, Wiley-VCH Verlag GmbH & Co. KGaA, Weinheim **2005**.

[44] a) W. G. Zumft, *Microbiol. Mol. Biol. Rev.* **1997**, *61*, 533. b) W. G. Zumft, *J. Mol. Microbiol. Biotechnol.* **2002**, *4*, 277.

[45] Since the cytoplasm of macrophages is more complex than the bacterial cytoplasm, it is reasonable to assume that displacement of Cu(II) in our experiments results from the reaction of the probe with NO•.

[46] PCMODEL 9.3; *Serena Software*, see: http://www.serenasoft.com/, **1988-2008**.

[47] J. Tao, J. P. Perdew, V. N. Staroverov, G. E. Scuseria, *Phys. Rev. Lett.* **2003**, *91*, 146401.

[48] a) S. Grimme, J. Antony, S. Ehrlich, H. Krieg, *J. Chem. Phys.* **2010**, *132*, 154104. b) S. Grimme, S. Ehrlich, L. Goerigk, *J. Comput. Chem.* **2011**, *32*, 1456.

[49] F. Weigend, S. Ahlrichs, *Phys. Chem. Chem. Phys.* **2005**, *7*, 3297.

[50] a) L. Goerigk, J. R. Reimers, *J. Chem. Theory Comput.* **2013**, *9*, 3240. b) M. Steinmetz, A. Hansen, S. Ehrlich, T. Risthaus, S. Grimme, *Top. Curr. Chem.* **2015**, *365*, 1.

[51] L. Goerigk, S. Grimme, *Wiley Interdiscp. Rev. Comput. Mol. Sci.* **2014**, *4*, 576.

[52] L. Goerigk, S. Grimme, *J. Chem. Theory Comput.* **2011**, *7*, 291.

[53] a) L. Goerigk, S. Grimme, *Phys. Chem. Chem. Phys.* **2011**, *13*, 6670. b) L. Goerigk, A. Hansen, C. Bannwart, S. Ehrlich, A. Najibi, S. Grimme, *Phys. Chem. Chem. Phys.* **2017**, *19*, 32184.

[54] F. Neese, *Wiley Interdiscp. Rev. Comput. Mol. Sci.* **2012**, *2*, 73.

[55] M. J. Frisch, G. W. Trucks, H. B. Schlegel, G. E. Scuseria, M. A. Robb, J. R. Cheeseman, G. Scalmani, V. Barone, B. Mennucci, G. A. Petersson, H. Nakatsuji, M. Caricato, X. Li, H. P. Hratchian, A. F. Izmaylov, J. Bloino, G. Zheng, J. L. Sonnenberg, M. Hada, M. Ehara, K. Toyota, R. Fukuda, J. Hasegawa, M. Ishida, T. Nakajima, Y. Honda, O. Kitao, H. Nakai, T. Vreven, J. A. Montgomery Jr., J. E. Peralta, F. Ogliaro, M. Bearpark, J. J. Heyd, E. Brothers, K. N. Kudin, V. N. Staroverov, T. Keith, R. Kobayashi, J. Normand, K. Raghavachari, A. Rendell, J. C. Burant, S. S. Iyengar, J. Tomasi, M. Cossi, N. Rega, J. M. Millam, M. Klene, J. E. Knox, F. B. Cross, V. Bakken, C. Adamo, J. Jaramillo, R. Gomperts, R. E. Stratmann, O. Yazyev, A. J. Austin, R. Cammi, C. Pomelli, J. W. Ochterski, R. L. Martin, K. Morokuma, V. G. Zakrzewski, G. A. Voth, P. Salvador, J. J. Dannenberg, S. Dapprich, A. D. Daniels, O. Farkas, J. B. Foresman, J. V. Ortiz, J. Cioslowski, D. J. Fox, *Gaussian 09, Revision B.01*, Gaussian, Inc., Wallingford CT **2010**.

[56] B. M. J. Tomasi, R. Cammi, *Chem. Rev.* **2005**, *105*, 2999.

SUPPORTING INFORMATION

Additional supporting information may be found online in the Supporting Information section at the end of the article.

How to cite this article: Barzegar Amiri Olia M, Hancock AN, Schiesser CH, Goerigk L, Wille U. Photophysical insights and guidelines for blue "turn-on" fluorescent probes for the direct detection of nitric oxide (NO•) in biological systems. *J Phys Org Chem*. 2018;e3896. https://doi.org/10.1002/poc.3896